Updated Calculation of Maximum Allowable Soil Concentrations for the Protection of Groundwater for Lead and Other Compounds Associated with Firearms at the Massachusetts Military Reserve

Arthur S. Rood and Laurence C. Hull

Idaho National Laboratory

April 11, 2007

1. INTRODUCTION

In support of the U.S. Environmental Protection Agency Region 1 (EPA I), the Idaho National Laboratory (INL) conducted a review of the draft document entitled *Environmental Assessment of Lead at Camp Edwards Massachusetts Small Arms Ranges* (Clausen et al, 2006) and calculated maximum soil concentrations of lead and other chemical compounds such that groundwater Maximum Contaminant Levels (MCL) would not be exceeded (Rood, 2007a). This report is essentially an update to the original report (Rood and Hull 2007) reflecting changes in parameter values based on a the February 15, 2007 meeting between the Army Corps of Engineers, US EPA Region 1, and State of Massachusetts, and other technical suggestions including uncertainty analysis that was originally reported in Rood 2007.

2. REVIEW OF ENVIRONMENTAL ASSESSMENT OF LEAD

The conceptual model presented does not seem complete, nor does it clearly define reservoirs and pathways. There would seem to be three reservoirs of lead in the soil,

1. lead slugs embedded in the backstop of firing ranges. This lead is present in relatively large particles with small surface area to mass ratio. This form of lead is likely fairly stable, and is the form of lead most discussed in this report.

2. lead released at the firing line from propellants or from abrasion on the bores of weapons. This lead would likely have left the weapon as an aerosol, and would be in the form of very fine particles. Because of heat, it is likely that this material is already oxidized. Lead in soil along the firing line, therefore, could be much more mobile than lead in the backstop.

3. lead abraded from slugs as they impact on the backstop. Small particles of lead would be abraded from the slugs. This lead would have a much higher surface area to mass ratio than the slugs, and would be expected to oxidize much more rapidly than the slugs.

Because the discussion is focused on slug lead, and does not address the two other sources of lead in the environment, which are both likely to be much more mobile than the slug lead, the report tends to underestimate the mobility of lead in the environment.

The conceptual model could be improved by presenting the pathway and mechanisms being considered. Three sources should be identified, as discussed above. The assumption that the slug lead and the abraded lead would oxidize to secondary mineral phases, such as cerusite, seem reasonable. However, no quantitative information on the rate of this corrosion is presented in a form relevant for the MMR. If corrosion is fast relative to recharge, lead concentrations will be high immediately around the slug, and localized mineral formation is likely. Infiltration would then leach the secondary mineral. Aqueous concentrations would be at or below the mineral saturation value depending on the rate of water movement relative to the rate of mineral dissolution. An alternative is possible in a humid environment with frequent precipitation. It is possible that infiltration would be faster than corrosion, and downward flushing of corrosion products would prevent water from reaching saturation with any lead mineral. Aqueous concentrations moving down would be lower than for mineral saturation. This is a case where corrosion of the slugs limits the release rate. The rate at which elemental lead, which will not be very mobile, is transformed to ionic lead, more mobile, would seem to be a key variable in predicting the mobility of lead.

It seems reasonable to assume that transport of lead will be limited by sorption to mineral grains. The U. S. Geological Survey has worked on the mobility of metals in groundwater at this site for many years. There is an extensive set of data and measurements to support conclusions of lead mobility in groundwater. One of the significant findings from the USGS work is that lead sorption significantly decreases between pH 6 and pH 4. Measured soil pH of 4.6 seems to indicate that sorption of lead could be inhibited in the vadose zone. The adsorption edge curves (change in lead sorption as a function of pH) are generally very steep, and therefore, very large changes in lead sorption could take place with very small changes in pH. It would seem that the site could have soil conditions that resulted in large variations in lead mobility. Because this seems such a sensitive parameter based on theoretical consideration of lead sorption by formation of surface complexes, the range of possible variation should be better constrained. Given the USGS studies, it is likely that site-specific surface complexation constants are available for the sedimentary material that could be used in a transport model. The sensitivity of lead mobility to pH changes could then be tested using the surface complexation model.

Lead measured in soil water in lysimeters was as high as 16 µg/L. Lead K_d values are given in EPA (1999) in table F.2. This table gives K_d values for different ranges of pH and concentrations of dissolved lead. The report quotes K_d values from Table F.2 for pH 4. to 6.3, which is appropriate for soils. However, the report quotes K_d values for dissolved lead less than 1 µg/L. A more appropriate range of K_d values to reference from the table would be 190 to 1900 mL/g for dissolved lead concentrations from 10 to 100 µg/L. If the USGS has measured lead sorption equilibrium constants, a geochemical code such as PHREEQC could be used to calculate K_d values as a function of pH and other soil chemical variables.

Overall, the report does not make a defensible case that lead is immobile in firing range soils.

1. Two forms of lead, which might be more mobile than the slugs of lead in the backstops, are not considered.

2. The mobility of lead as a function of pH is not fully evaluated. This is important because the reported soil pH of 4.6 is in a range of the lead sorption isotherm that is very sensitive to small changes in pH. Large changes in lead mobility could occur for small changes in pH for this region of the sorption isotherm.

3. The relative rates of elemental lead corrosion and recharge are not evaluated. These rates are needed to quantify the source release rate of lead. For lead near the firing lines, the lead could be deposited in a mobile form and be released much more rapidly than elemental lead in slugs.

4. Numerical calculations of lead release and transport could be conducted with readily available computer codes including Hydrus, CXTFIT, MCM, GWSCREEN, or PHREEQC. This would provide a means of collecting the different variables and testing the sensitivity of lead mobility. Such an assessment would provide a better argument for lead mobility or lack of mobility.

5. The report implies that once sorbed in the vadose zone, lead will be immobile. Sorption only slows down the rate of lead movement, it does not stop it. If lead is allowed to corrode, and is leached below the backstops, subsequent treatment of the backstops will not remediate the lead that has already been released. Lead will then continue to move downward to groundwater over time.

3. MAXIMUM ALLOWABLE SOIL CONCENTRATIONS OF LEAD AND OTHER CHEMICAL COMPOUNDS

The primary focus of this work was to establish maximum concentrations of lead and other chemical compounds in soil such that after leaching and transport in the vadose zone, chemical concentrations in the aquifer would not exceed their Maximum Contaminant Limit (MCL). These calculations were to focus on the Echo and Tango firing ranges at the MMR and include the chemical compounds lead (MCL=0.015 mg/L), antimony (MCL=0.006 mg/L), nitroglycerin (MCL=0.0048 mL/g), and 2-4-dinitrotoluene (24DNT) (MCL=0.073 mL/g). Because of the importance placed on lead, additional work was performed to calibrate the transport model to measured concentration profiles of lead in soil. The calibration parameter was the lead equilibrium sorption coefficient (*Kd*).

3.1 Calibration of Lead *Kd*

Soil sampling for lead and other constituents that was performed in 2002 and 2006 at the Echo and Tango Ranges was used to estimate an *effective Kd* value for lead in MMR soils. The calibrated *Kd* value may represent many processes other than sorption, such as colloid transport. It is beyond the scope of this report to speculate on the dominant process; rather, the *Kd* combined with the estimated infiltration rate and moisture content is used to describe bulk movement of lead in soils as observed in soil profiles at the Echo and Tango firing sites.

The depth distribution of lead in soils was examined from the soil profile samples taken at the firing points. Samples taken at the firing backstop would not be appropriate because the soil is disturbed when the projectile hits the backstop. Firing point samples were used because the lead in the soil would come from deposition of small, aerosol particles that are emitted from the barrel and firing chamber when a weapon is discharged. These small particles will deposit on the soil surface from air and will more readily dissolve for reasons stated in Section 2. The following assumptions were made for lead *Kd* calibration:

1. Lead is deposited from air on the ground surface at the firing point.

2. The ground where lead deposits is relatively undisturbed.

3. Lead deposition is assumed to be constant from the time the ranged opened to the time samples were taken.

Table 1 lists the primary data used for lead *Kd* calibration. In several cases (samples 169C C1, 169C D3, 169A C1) the lead profile showed a bimodal distribution of concentration with depth, Lead concentrations in the 15-30 cm depth range were higher than lead concentrations in the 7.5 to 15 cm depth. This profile suggests two periods of input to the soil column or other process that moved a quantity of lead past the 7.5 to 15 cm layer. In these cases (labeled alternate depth range), the inventory in the 0 to 7.5 cm and 7.5 to 15 cm depths were added together so than the model was calibrated to two layers; 0 to 15 cm and 15 to 30 cm.

The lead loading rate to the soil surface is unknown and for this reason, the calibration "target" was the ratio of the lead inventory in the 0 to 7.5 cm layer to the lead inventory in a subsequent layer. This ratio was termed the inventory ratio and is given by Equation (1).

Table 1. Lead concentrations in soil profiles taken at Tango and Echo range. All samples were taken in 2002 except for the Area 1 CS (Center South) which was taken in 2005.

Range	Sample ID	Top (m)	Bottom (m)	Cell Thickness (m)	Soil Mass (kg m^{-2})	Lead Conc (mg kg^{-1})	Lead Mass (mg m^{-2})	Alternate Depth Ranges (m)	Lead Mass for Alternate Depth (mg m^{-3})	Ratio of inventory in surface layer
Tango	169B D3	0	0.0762	0.0762	131.1	345	4.52E+04			1.00
Tango	196B D3	0.0762	0.1524	0.0762	131.1	111	1.45E+04			0.32
Tango	169B D3	0.1524	0.3048	0.1524	262.1	20.7	5.43E+03			0.12
					Total		6.52E+04			
Tango	169B C1	0	0.0762	0.0762	131.1	195	2.56E+04			1.00
Tango	169B C1	0.0762	0.1524	0.0762	131.1	57.9	7.59E+03			0.30
					Total		3.31E+04			
Tango	169C C1	0	0.0762	0.0762	131.1	394	5.16E+04	0-0.15	6.78E+04	1.00
Tango	169C C1	0.0762	0.1524	0.0762	131.1	123	1.61E+04	0.15-0.30	4.95E+04	0.73
Tango	169C C1	0.152	0.305	0.152	262.1	189	4.95E+04			
					Total		1.17E+05			
Tango	169C D3	0.000	0.076	0.076	131.1	483	6.33E+04	0-0.15	6.75E+04	1.00
Tango	169C D3	0.076	0.152	0.076	131.1	31.9	4.18E+03	0.15-0.30	3.56E+04	0.53
Tango	169C D3	0.152	0.305	0.152	262.1	136	3.56E+04			
					Total		1.03E+05			
Tango	Area1 CS	0.000	0.076	0.076	131.1	386	5.06E+04			1.00
Tango	Area1 CS	0.229	0.305	0.076	131.1	100	1.31E+04			0.26
					Total		6.37E+04			
Tango	169A C1	0.000	0.076	0.076	131.1	540	7.08E+04	0-0.15	1.07E+05	1.00
Tango	169A C1	0.076	0.152	0.076	131.1	276	3.62E+04	0.15-0.30	6.71E+04	0.63
Tango	169A C1	0.152	0.305	0.152	262.1	256	6.71E+04			
					Total		1.74E+05			
Echo Range	159A C1	0.000	0.076	0.076	131.1	142	1.86E+04			1.00
Echo Range	159A C1	0.076	0.152	0.076	131.1	33	4.33E+03			0.23
					Total		2.29E+04			

$$IR_i = \frac{INV_1}{INV_i} \quad (1)$$

Where

INV_1 = lead inventory in the first (surface) layer (mg)

INV_i = lead inventory in layer *i* (surface or subsurface) (mg)

IR_i = inventory ratio for layer *i*

The lead inventory in the i^{th} layer was calculated by

$$Q_i = C_i \times \rho \times A \times T_i \quad (2)$$

Where

Q_i = lead inventory in the i^{th} layer (mg)

C_i = lead concentration in i^{th} soil layer (mg kg^{-1})

ρ = bulk density (1720 kg m^{-3})

T_i = thickness of the i^{th} layer (m)

A = unit area (1 m^2)

The bulk density value was taken from Soil Screening Level spreadsheet produced in 2001 for EPA Region 1 by A. S. Rood of the Idaho National Laboratory as reported in AMEC 2001.

The Mixing Cell Model (MCM) (Rood 2004; Rood 2005) was used to compute lead transport in the soil. The MCM model is a one dimensional flow and transport code for the unsaturated zone. The code requires input of water and contaminant fluxes into the uppermost cell. First-order differential equations describe the mass balance of water and contaminant in each of the cells that make up the modeling domain. Output from the model includes water and contaminant inventories, contaminant concentrations, and water and contaminant fluxes. For calibration, a unit release rate (1 mg yr^{-1}) over the time the firing range began operation to the time the measurement was made was assumed. The *Kd* was calibrated by matching the predicted and observed inventory ratios as described in Equation 1.

Infiltration was based on monthly precipitation records from the Blue Hill Massachusetts recording station. The fraction of precipitation that infiltrates was based on data in Clausen et al. 2006 which states an annual average precipitation of 48 in yr^{-1} and an annual average infiltration of 27 in yr^{-1}. Therefore, the fraction of precipitation that infiltrates is 27 in/48 in = 0.5625. The fraction of precipitation that infiltrates was multiplied by each monthly precipitation record to arrive at a monthly infiltration value (Figure 1).

Moisture content in the soil was determined using van Genuchten (1980) fitting parameters that were calibrated to the moisture profile data in AMEC 2004. The calibrated fitting parameters results in a moisture content of 0.12 for an annual infiltration of 0.685 m. Figure 2 shows the calibrated moisture characteristic curve and several other moisture characteristic curves for various soil types using van Genuchten fitting parameters published in Carsel and Parrish (1988) (Table 2).

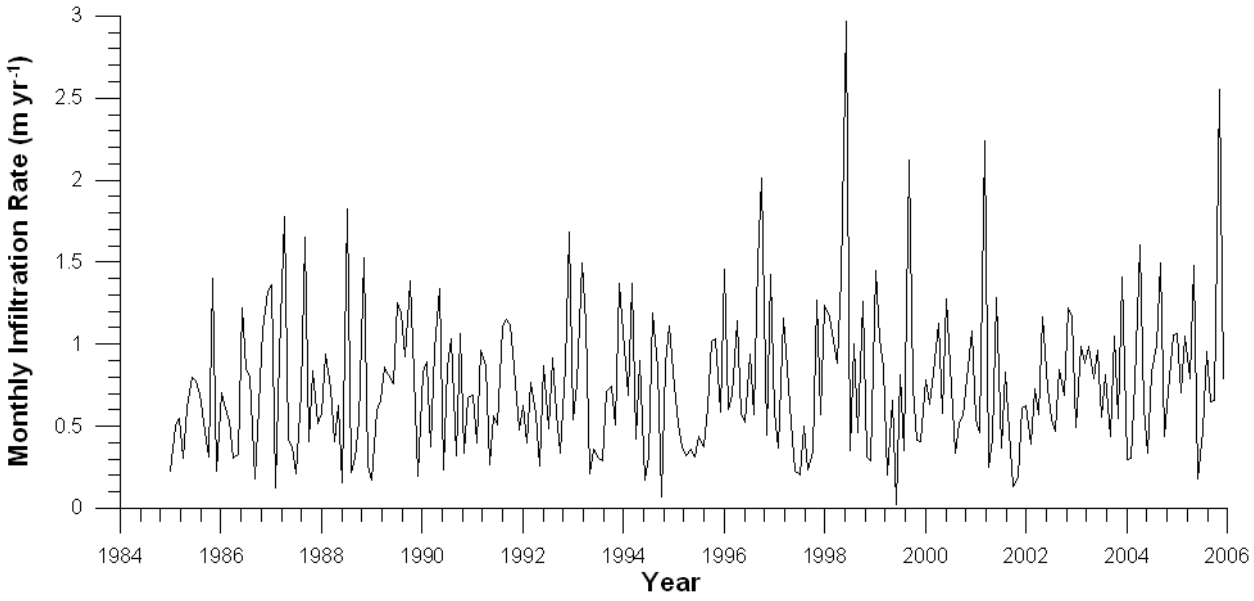

Figure 1. Monthly infiltration rate used to calibrate lead *Kd* value to soil concentration profiles.

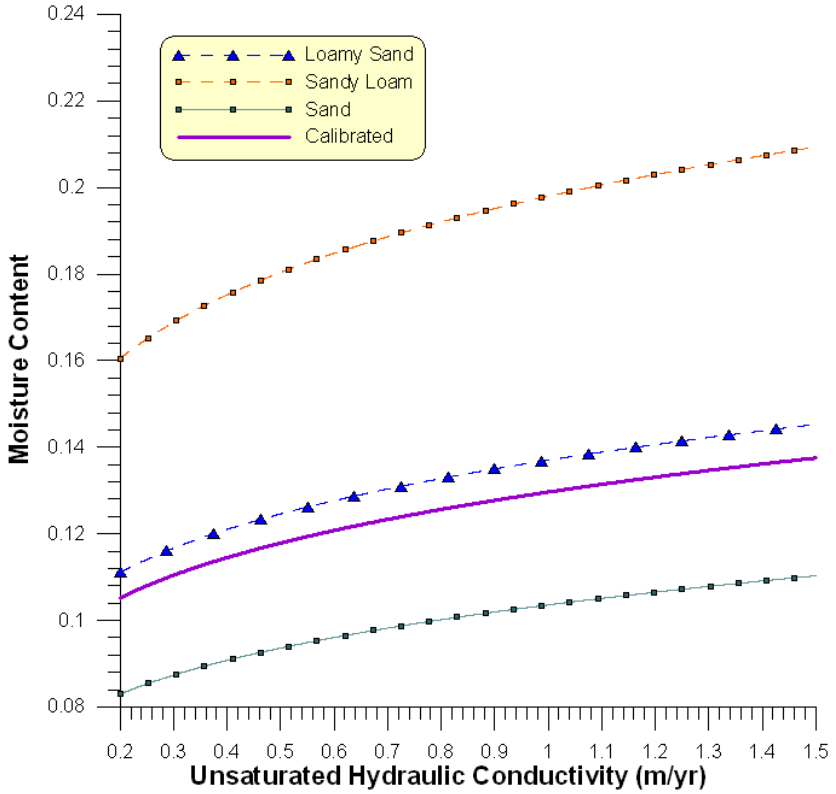

Figure 2. Moisture characteristic curves for various lithologies using the van Genuchtem (1980) fitting parameters from Carsel and Parrish (1988) and a curve calibrated to moisture data in AMEC 2004.

Table 2. Mean representative values of the saturated hydraulic conductivity (K_{sat}), residual moisture content (θ_r), saturated moisture content (θ_s), and the van Genuchten fitting parameters α and n for various soil types (from Carsel and Parrish 1988) and calibrated from data in AMEC 2004.

Soil Type	Percent sand	Percent clay	n	α (cm^{-1})	θ_r	θ_s	K_{sat} ($cm\ yr^{-1}$)
Loamy sand	80.9	6.4	2.28	0.124	0.057	0.41	127,808
Sand	92.7	2.9	2.68	0.145	0.045	0.43	260,172
Sandy loam	63.4	11.1	1.89	0.075	0.065	0.41	38,719
Calibrated	n/a	n/a	2.45	0.13	0.057	0.41	127,800

A calibrated *Kd* value was calculated for each soil profile (Table 3 and Figure 3). The distribution of calibrated *Kd* values had a mean of 69 mL g^{-1} with a standard deviation of 63 mL g^{-1}. The geometric mean *Kd* value was 47 mL g^{-1} and the geometric standard deviation was 2.6. Recent measurements of the lead *Kd* in MMR soils (Larsen et al. 2007) report a value of 34 mL g^{-1}, which is in general agreement with the geometric mean *Kd* value of 47 mL g^{-1} cited above from calibration to soil profiles. For calculation of maximum allowable soil lead concentrations, a geometric mean *Kd* value of 47 was used because lognormal statistics are preferable with the distribution spans over an order of magnitude.

Table 3. Calibrated lead *Kd* values for Echo and Tango ranges.

Sample	Calibrated Kd (mL g^{-1})
169B D3	100
169B C1	100
169C C1	15
169C D3	27
Area 1 CS	35
169A C1	20
159A C1	185
Average	69
Standard Deviation	63
Geometric Mean	47
Geometric Standard Deviation	2.6

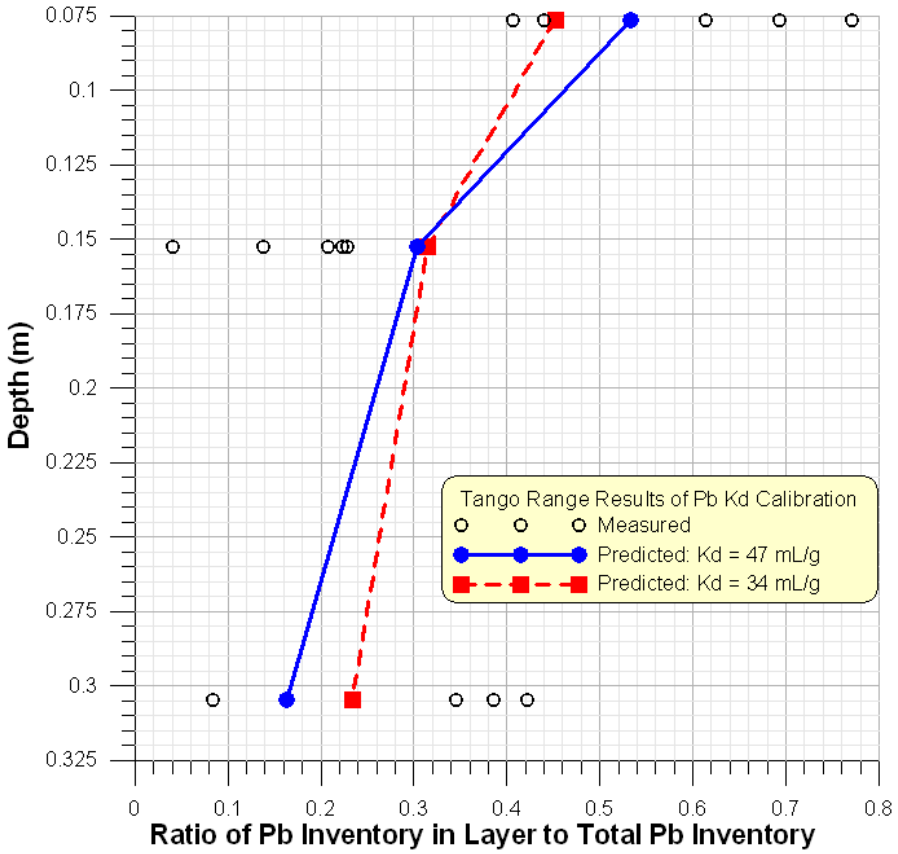

Figure 3. Predicted and measured ratio of the lead inventory in a given layer to the total lead inventory in the profile for Tango Range firing line soils.

The data in Table 3 were also analyzed using the ProUCL software (EPA 2004). ProUCL is used to calculate the upper confidence limit (UCL) on the mean of a distribution of environmental data and contains many statistical algorithms to test the input distribution against various analytical distributions in addition to non-parametric tests. In this case, we are interested in the lower confidence limit (LCL) of the mean Kd value. The data set was tested and found to be normal and lognormal at the 5% significance level (There were no recommended distributions at the 2% significance level). The UCL of the mean was 114.93 mL/g assuming a normal distribution. Because the normal distribution is symmetrical, the LCL can be calculated as

$$LCL = \bar{x} - \left(UCL - \bar{x}\right) = 2\bar{x} - UCL = 2(68.86) - 114.93 = 22.8\ \text{mL/g}$$

Therefore, a bounding *Kd* of 22.8 mL/g could also be used as a basis for defining maximum allowable soil concentrations.

3.2 Calculation Methodology

Maximum allowable soil concentrations (*MASC*) for groundwater protection should consider site specific variables such as depth to groundwater, area of the contaminated region, and orientation of the contaminated region relative to groundwater flow. Because the orientation and area of each source may

vary from site to site, a more general methodology was developed using fitting equations such that the *MACS* for any area source could be determined without having to rerun the model.

Allowable soil concentrations were only calculated for the firing sites. Target backstops would likely have an allowable soil concentration that is higher because lead bullets and slugs would have to corrode first before leaching and transport could occur. Therefore, these *MASC* values should be bounding for the target backstop regions.

Table 4 lists the unsaturated and aquifer parameters used in the simulation. The MCM (Rood 2005) code was used to compute unsaturated transport and the GWSCREEN (Rood 1999) code was used to compute groundwater concentrations and maximum allowable contaminant *mass* in soil (in mg). The MASC was calculated by dividing the maximum allowable contaminant mass in soil (mg) by the mass of soil that is contaminated (kg).

A contaminant mass of 1 mg was run for each contaminant and case. The maximum allowable soil concentration was calculated by

$$MASC = \frac{\frac{MCL}{C_{\max}}}{L \times W \times T \times \rho} \tag{3}$$

Where

$MASC$ = maximum allowable soil concentration (mg/kg)

MCL = maximum concentration limit of the contaminant in aquifer (mg/L)

$C_{\max}$ = maximum aquifer concentration for 1 mg initial inventory (mg/L)

ρ = bulk density (1720 kg m^{-3})

L = length of source (m)

W = width of source (m)

T = thickness of source (0.368 m)

Table 4. Parameter values used to calculate maximum allowable soil concentrations

Parameter	Value	Units	Comments
Unsaturated thickness	36.8	m	unsaturated thickness at Tango range (oral comm. L. Cain)
Number of cells	100	n/a	user discretion
Cell thickness	0.368	m	unsaturated thickness/number of cells
Moisture content	0.123	m^3/m^3	calculated from calibrated moisture characteristic curves
Area of source (Case 1)	100	m^2	assumed - user discretion
Area of source (Case 2)	400	m^2	assumed - user discretion
Area of source (Case 3)	1600	m^2	assumed - user discretion
Area of source (Case 4)	6400	m^2	assumed - user discretion
Bulk density	1.72	g/cm^3	USACE 2007
Darcy velocity in aquifer	37	m/yr	USACE 2007
Porosity (aquifer)	0.35	m/m	Average from USACE 2007 and AMEC 2001
Longitudinal dispersivity	10	m	McTigue, oral comm. 2007
Transverse dispersivity	2	m	McTigue, oral comm. 2007
Vertical dispersivity	0.0116	m	McTigue, oral comm. 2007
Dispersivity in unsaturated zone	2	m	assumed
Porosity	0.4	m^3/m^3	USACE 2007
Infiltration rate	0.685	m/yr	based on annual infiltration of 27 in/yr
Kd, lead	47	mL/g	calibrated
Kd Nitroglycerin, surface [a]	1.94	mL/g	Speitiel and Yamamoto (2002)
Kd Nitroglycerin, to 3 m depth [a]	0.617	mL/g	Speitiel and Yamamoto (2002) and EDMS DB
Kd Nitroglycerin, 3–30 m [a]	0.0536	mL/g	Speitiel and Yamamoto (2002) and EDMS DB
Kd Nitroglycerin, >30 m [a]	0.0634	mL/g	Speitiel and Yamamoto (2002) and EDMS DB
Kd 24DNT surface [a]	3.11	mL/g	Speitiel and Yamamoto (2002)
Kd 24DNT to 3 m depth [a]	0.99	mL/g	Speitiel and Yamamoto (2002) and EDMS DB
Kd 24DNT, 3–30 m [a]	0.086	mL/g	Speitiel and Yamamoto (2002) and EDMS DB
Kd 24DNT, >30 m [a]	0.102	mL/g	Speitiel and Yamamoto (2002) and EDMS DB
Kd antimony	45	mL/g	SSL spreadsheet

a. *Kd* based on fraction of organic carbon (foc) provided in an email from M. Kulbersh: 0-1 ft, foc=1.194%, 1-10 ft, foc=0.38%, 10-100 ft, foc=0.033%, >100 ft, foc = 0.039%

The source length parallel to groundwater flow and width perpendicular to groundwater flow were identified as potentially important site-specific parameters. A source elongated perpendicular to groundwater flow will have a higher *MASC* compared to a source of equivalent area elongated parallel to groundwater flow. The sensitivity of the *MASC* to source width is dependent on the transverse dispersivity in the aquifer because this parameter determines the amount of lateral plume spreading.

To address the sensitivity of the *MASC* to the width of the source perpendicular to groundwater flow and the transverse dispersivity, several GWSCREEN (Rood 1999) simulations were run. These computations (Table 5) revealed that the *MACS* values were relatively insensitive to the width of the source when the

nominal value of the transverse dispersivity is used (0.0914 m). When the transverse dispersivity was increased to 1.5 m, the *MACS* values were generally more sensitive to the width of the source.

Because the transverse dispersivity in the aquifer is small, the width of the source is not an important parameter, and only the length of the source parallel to groundwater flow needs to be considered. Therefore, the regression equation for the *MASC* as a function of area of the source was provided in terms of the length of the source parallel to groundwater flow. The general equation for the *MASC* is given by

$$MASC = a\left(L^2\right)^b \tag{4}$$

where a and b are fitting parameters and L is the length of the source parallel to groundwater flow (m).

Table 5. Sensitivity of the *MACS* to width of source perpendicular to groundwater flow and transverse dispersivity.

Transverse dispersivity (m)	Width (m)	Length (m)	Area (m^2)	Maximum concentration for a 1 mg source (mg/m^3)	Limiting Inventory (mg)	MASC (mg/kg)
9.14E-02	1.00E+01	4.00E+01	4.00E+02	1.37E-07	1.10E+08	6.42E+02
9.14E-02	1.00E+02	4.00E+01	4.00E+03	1.42E-08	1.06E+09	6.21E+02
1.5	1.00E+01	4.00E+01	4.00E+02	7.11E-08	2.11E+08	1.24E+03
1.5	1.00E+02	4.00E+01	4.00E+03	1.42E-08	1.06E+09	6.21E+02
9.14E-02	4.00E+01	4.00E+01	1.60E+03	3.54E-08	4.24E+08	6.20E+02
1.5	4.00E+01	4.00E+01	1.60E+03	3.41E-08	4.39E+08	6.44E+02

3.3 Results

Maximum allowable soil concentrations for lead, antimony, nitroglycerin, and 24DNT are shown in Table 6. The values can be thought of as the mass of contaminant that is evenly dispersed within a soil volume defined by the modeled area and thickness of the source. The thickness of each source was defined by the cell thickness of 0.368 m.

Table 6. Maximum allowable soil concentrations for lead and other contaminants (mg/kg) in a 0.368 m thick source.

Contaminant	Case 1 (100 m^2)	Case 2 (400 m^2)	Case 3 (1600 m^2)	Case 4 (6400 m^2)
Pb	1930	980	520	290
Nitroglycerin	2.0	1.0	0.55	0.31
Antimony	740	380	200	110
24DNT	44	22	12	6.6

The data in Table 6 was fit to a power function so that the limiting soil concentration from any area source can be determined (Figures 4 thru 7 and Table 7).

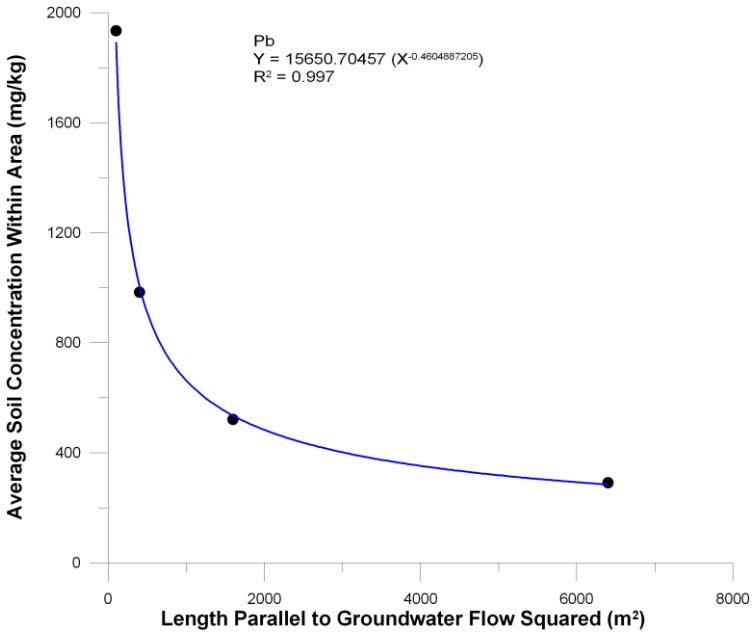

Figure 4. Power function fit for lead of the area of a square source to the maximum allowable soil concentration for a *Kd* of 47 mL/g and source thickness of 0.368 m.

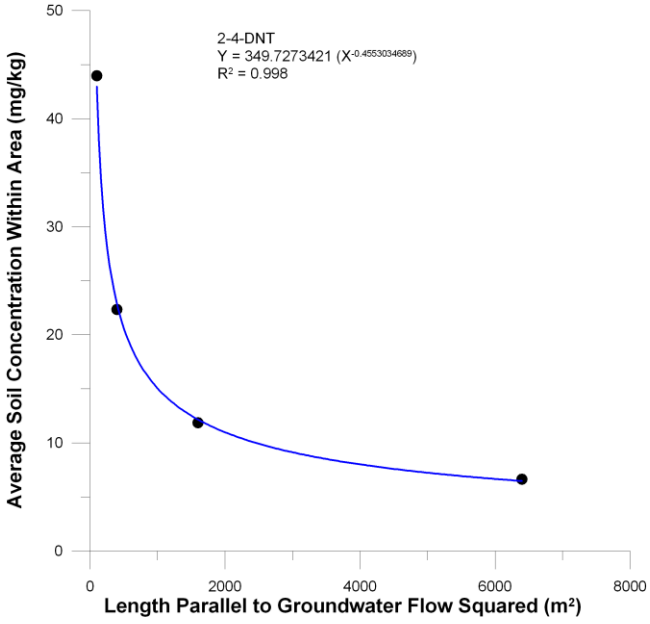

Figure 5. Power function fit for 24DNT of the area of a square source to the maximum allowable soil concentration for source thickness of 0.368 m.

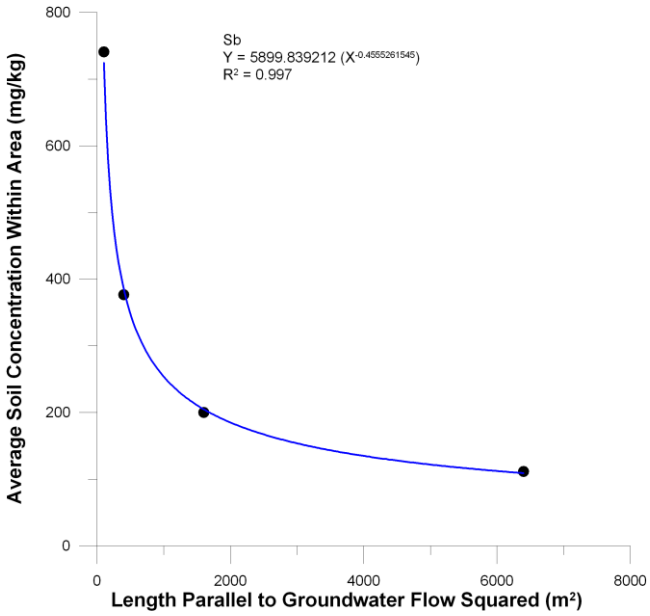

Figure 6. Power function fit for antimony of the area of a square source to the maximum allowable soil concentration for source thickness of 0.368 m.

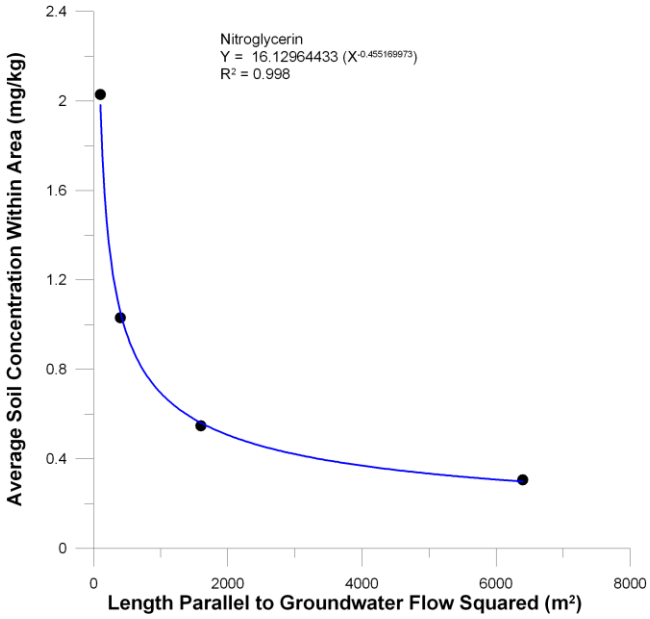

Figure 7. Power function fit for nitroglycerin of the area of a square source to the maximum allowable soil concentration for source thickness of 0.368 m.

Table 7. Fitting parameters for power function fit to the MASC value as a function of the length of the source parallel to groundwater flow squared (see Equation 4).

Fitting Parameter	Lead	Nitroglycerin	Antimony	2-4-DNT
a	-0.46048873	-0.45516997	-0.45552615	-0.45530347
b (mg/kg)	15650.7	16.12964433	5899.83	349.7273421

The pore water concentration at 5 feet such that the concentration in groundwater would not exceed the MCL was calculated using MCM (Table 8). This concentration (termed the critical pore water concentration) may be used as a trigger level to either cease operations or initiate clean up. In general, the pore water concentration decreases with increasing area of the source. Critical pore water concentrations for were independent of *Kd*.

Table 8. Critical pore water concentrations at 5 feet.

(Length of source)^2 (m^2)	Pb (mg/L)	Sb (mg/L)	Nitroglycerin (mg/L)	24DNT (mg/L)
100	5.9	2.4	0.30	4.2
400	3.0	1.2	0.15	2.1
1600	1.6	0.64	0.082	1.1
6400	0.90	0.36	0.046	0.64

Contaminant fluxes to the groundwater for a unit (1 mg) mass in the source area are plotted in Figures 9 and 10. Contaminant fluxes were calculated using the MCM code (Rood 2005). The arrival of the leading edge of the contaminant plume for lead and antimony was around 1000 years. This arrival time may be shortened by increasing the longitudinal dispersivity in the unsaturated zone.

Groundwater concentrations for the 10 m × 10 m source are plotted in Figure 11. The groundwater concentrations were calculated with GWSCREEN (Rood 1999) using the contaminant fluxes to the aquifer that are shown in Figure 9 and 10. Since none of the contaminants decay with time, the primary difference between the curves is reflected in the *Kd* value. Note that the maximum contaminant concentration is inversely related to the *Kd* value and the *time* of maximum concentration is directly related to the *Kd* value.

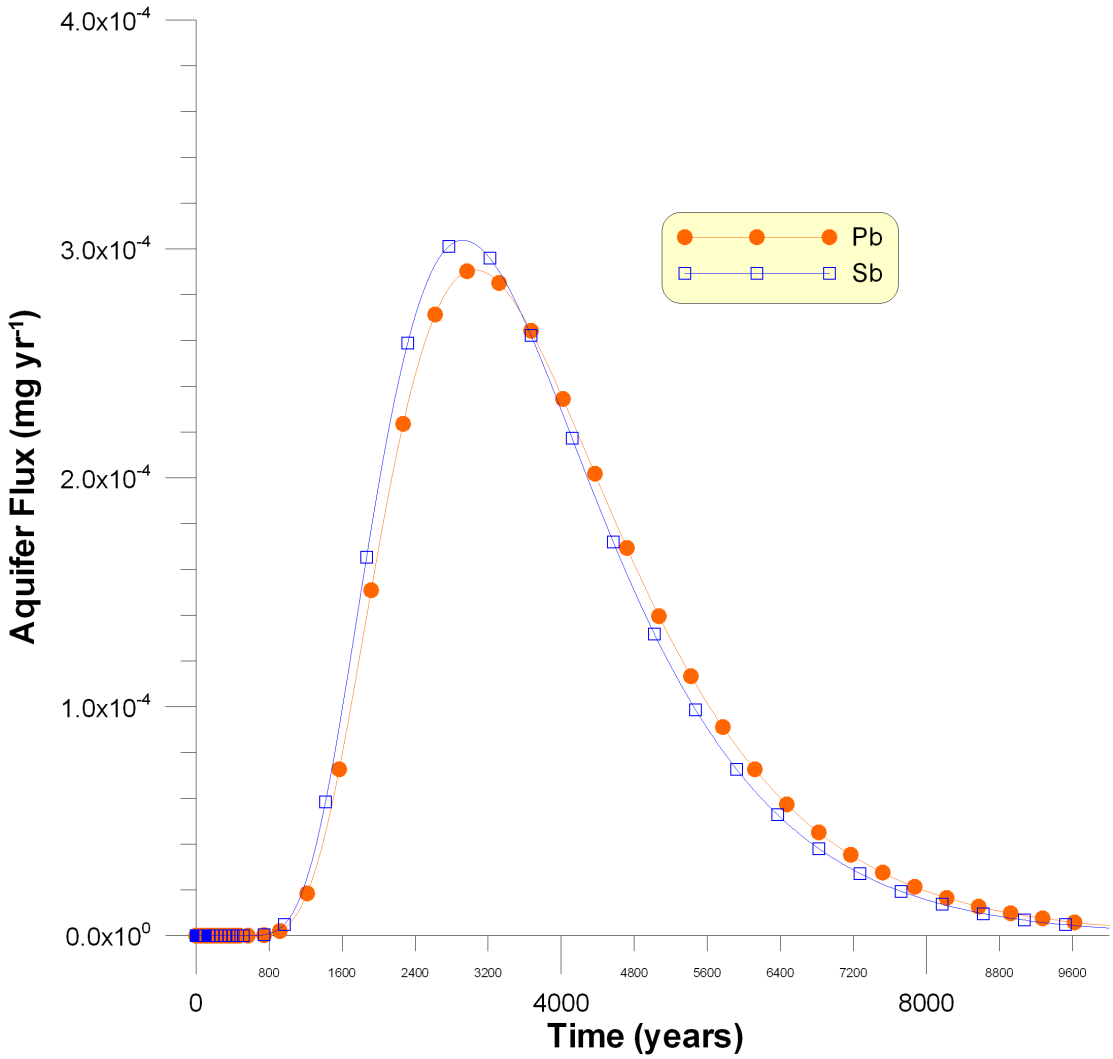

Figure 8. Lead and antimony fluxes to the groundwater as a function of time for a 1 mg source mass.

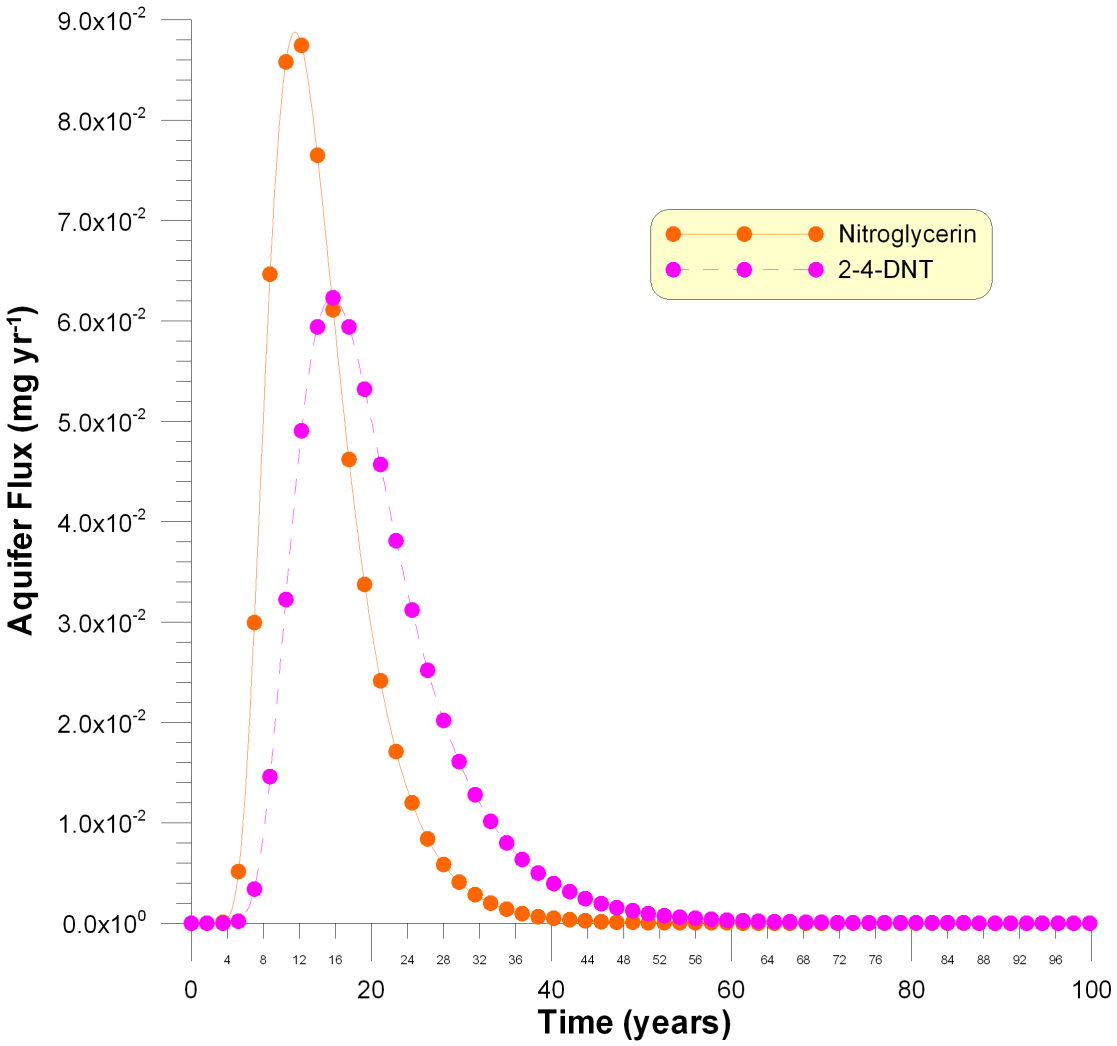

Figure 9. Nitroglycerin and 2-4-DNT fluxes to the groundwater as a function of time for a 1 mg source mass.

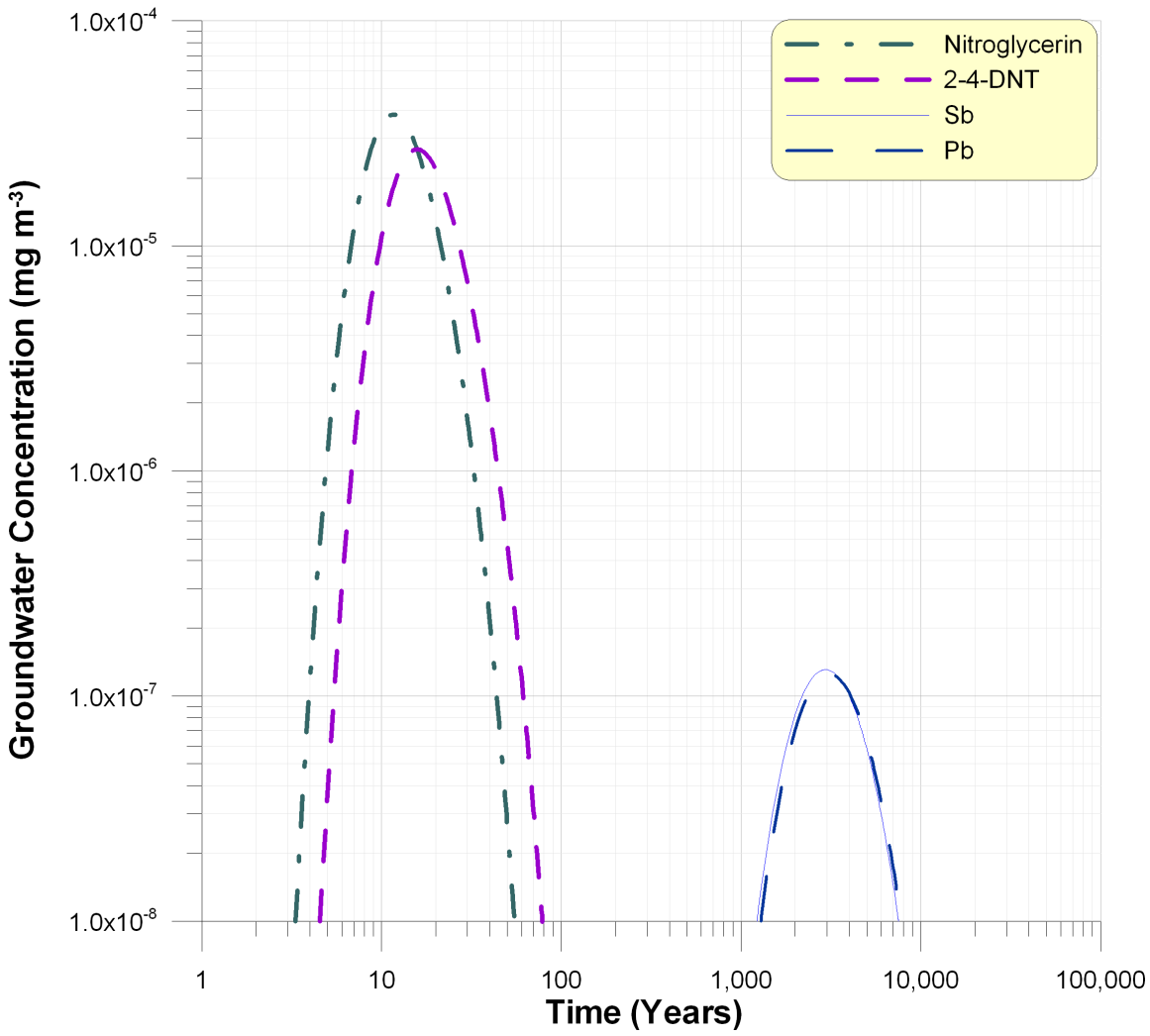

Figure 10. Concentration as a function of time for a 10 m × 10 m source and initial contaminant mass of 1 mg in the unsaturated zone.

3.4 Application of Methodology

In this section, the methodology applied to the Tango and Echo Ranges to demonstrate how the maximum allowable concentrations may be applied to a site. Ten sampling grids were defined at the Tango Range and 13 sampling grids for the Echo Range. For each sampling grid, composite samples were taken which provides an average concentration across the area of the sample grid. For lead and antimony, sampling was performed to a 1 ft (0.3048 m) depth. For nitroglycerin, sampling depth was 3 inches (0.0762 m). The modeling results were based on a source depth of 0.368 m and must be adjusted to the actual sampling depth from the measured data. The *MASC* value is adjusted for actual sampling depth by:

$$MASC(x) = MASC(0.368\ \text{m}) \times \frac{0.368\ \text{m}}{x} \tag{5}$$

where *MASC* (*x*) is the maximum allowable soil concentration adjusted for sampling depth of *x* meters, and *MASC* (0.368 m) is the maximum allowable soil concentration for a contamination thickness of 0.368 m.

The length of each sampling region parallel to groundwater flow was obtained from Figure 1 in USACE 2006a for the Tango Range and Figure 3-3 in USACE 2006b for the Echo Range. The length was estimated by determining the length of the longest line segment parallel to groundwater flow that traversed the sampling region. The area of each sampling region was determined from GIS shape files provided by Mathew Walsh of USACE.

Lead concentrations in sampling region 1 E of the Tango Range are used as an example to demonstrate the methodology (Table 9). The length of sampling region 1 E was estimated from Figure 1 in USACE 2006a to be 50.4 m. The length is squared as shown below.

$(50.44\ \text{m})^2 = 2544\ \text{m}^2$.

Using the *MASCs* power function fit for lead (Figure 4) gives a lead *MASC* value of

$(15650.7\ \text{mg/kg} \times (2544\ \text{m}^2)^{0.460488725}) = 423\ \text{mg/kg}$.

The MASC value is then corrected for the sampling depth

$423\ \text{mg/kg} \times 0.368\ \text{m}/0.3048\ \text{m} = 511\ \text{mg/kg}$

The measured concentration in sampling region 1 E was 87.4 mg/kg (Table 9). Therefore, the measured concentration of sampling region 1 E is less than the *MASC* value and the existing lead in soil is not expected to pose a threat to groundwater.

Each sampling region is evaluated in a similar manner. The last step is to evaluate to composite of all the sampling regions. In this step, the area-weighted measured concentration is calculated for the composite region. The composite region includes all the sampling regions that comprise the firing range. The area-weighted measured concentration (C_{WT}) is given by

$$C_{WT} = \left(\sum_i C_i \frac{A_i}{\sum_i A_i} \right) \tag{6}$$

where C_i is the concentration from the i^{th} sampling region (mg/kg), and A_i is the area if the i^{th} sampling region (m^2).The length of the composite region parallel to groundwater flow was determined in a similar manner to the length parallel to groundwater flow for each individual sampling region.

Returning to the previous example, the depth-corrected *MASC* value for the Tango composite region was 144 mg/kg. The area-weighted measured concentration (98.1 mg/kg) is less than the depth-corrected *MASC* value for the entire area and therefore, existing lead in soil at the Tango Range is not expected to pose a threat to groundwater.

It should be noted that the area-weighted average is really a means at obtaining the integrated mass of lead in the entire region. Thus

$$M = \iiint_{x,y,z} C(x,y,z)\rho(x,y,z)\,dx\,dy\,dz \cong \sum_{i=1}^{n} C_i \rho_i A_i T_i \qquad (7)$$

where M is the total mass in the region, C_i is the contaminant concentration (mg/kg) in sub-region i, ρ_i is the bulk density in sub-region i (kg/m^3), A_i is the area of sub-region i, T_i is the thickness of sub-region i, and n is the number of sub-regions that comprise the total region. The average concentration in the total region is obtained by dividing M by the total soil mass in the region. Equation 7 may be more flexible to use because it takes into account differences in sampling depth and bulk density from sub-region to sub-region.

Table 9 thru 12 present a comparison the *MASC* values to measured concentrations for lead, antimony, nitroglycerin, and 2-4-DNT for the Tango and Echo Range sampling regions and composite for the entire range. The column labeled "Meas/*MASC*" is the ratio of the measured concentration to the MASC value. If this ratio is greater than 1, then the *MASC* value was exceeded. Measured data for 2-4-DNT were not found in USACE 2006a and 2006b, so only the *MASC* values are presented for this compound.

The MASC value was exceeded for nitroglycerin in the Tango Range (sampling region 1 C-N) and for the composite of the entire range.

Table 9. Lead *MASC* values for Tango and Echo Ranges.

Range	Sampling Grid ID	Length Parallel to GW Flow Squared (m^2)	Length Parallel to GW Flow (m)	Area of sampling grid (m^2)	Measured Concentration (mg/kg)	*MASC* (mg/kg)	*MASC* (depth corrected) (mg/kg)	Meas/*MASC*	Area-weighted measured concentration (mg/kg)
Tango	1 E	2544	50.44	1180	87.4	423	511	0.171	5.4
Tango	1 C-N	635.4	25.2	575	461	801	967	0.477	14.0
Tango	1 C-S	574.0	24.0	650	386	840	1014	0.381	13.3
Tango	1 W	2232.0	47.2	1328	180	449	542	0.332	12.6
Tango	2 E	248.3	15.8	305	78.3	1235	1491	0.053	1.3
Tango	2 C	248.3	15.8	306	123	1235	1491	0.082	2.0
Tango	2 W	248.5	15.8	306	131	1235	1491	0.088	2.1
Tango	3 E	12174.4	110.3	4578	82.5	206	248	0.332	20.0
Tango	3 C	8928.0	94.5	4766	66.2	237	286	0.231	16.7
Tango	3 W	5395.9	73.5	4936	41.4	299	361	0.115	10.8
Tango	Total	39857.7	199.6	18931		119	144	0.682	98.1
Echo	1 N	89.3	9.4	267	70.4	1978	2388	0.029	2.95
Echo	1 C	89.3	9.4	244	12.7	1978	2388	0.005	0.49
Echo	1 S	89.3	9.4	250	17	1978	2388	0.007	0.67
Echo	2 N	916.1	30.3	980	34	677	817	0.042	5.23
Echo	2 C	985.6	31.4	894	26.4	655	790	0.033	3.70
Echo	2 S	985.6	31.4	916	23	655	790	0.029	3.30
Echo	3 N	192.3	13.9	445	68.2	1389	1677	0.041	4.77
Echo	3 C	192.3	13.9	406	90.8	1389	1677	0.054	5.79
Echo	3 S	175.0	13.2	416	68.2	1451	1752	0.039	4.45
Echo	4 N	268.9	16.4	446	264	1191	1437	0.184	18.48
Echo	4 S	636.2	25.2	1110	555	801	967	0.574	96.64
Echo	5 SP1	101.8	10.1	80	140	1862	2248	0.062	1.75
Echo	5 SP2	142.0	11.9	113	170	1597	1928	0.088	3.00
Echo	Total	6088.5	78.0	6375		283	342	0.443	151.23

Table 10. Nitroglycerin *MASC* values for Tango and Echo Ranges.

Range	Sampling Grid ID	Length Parallel to GW Flow Squared (m^2)	Length Parallel to GW Flow (ft)	Area of sampling grid (m^2)	Measured Concentration (mg/kg)	*MASC* (mg/kg)	*MASC* (depth corrected) (mg/kg)	Meas/*MASC*	Area-weighted measured concentration (mg/kg)
Tango	1 E	2544.6	50.4	1180		0.454	2.195	0.000	0.000
Tango	1 C-N	635.4	25.2	575	26	0.855	4.127	6.300	0.790
Tango	1 C-S	574.0	24.0	650	3.2	0.895	4.323	0.740	0.110
Tango	1 W	2232.0	47.2	1328		0.482	2.330	0.000	0.000
Tango	2 E	248.3	15.8	305		1.311	6.330	0.000	0.000
Tango	2 C	248.3	15.8	306		1.311	6.330	0.000	0.000
Tango	2 W	248.5	15.8	306		1.310	6.327	0.000	0.000
Tango	3 E	12174.4	110.3	4578		0.223	1.076	0.000	0.000
Tango	3 C	8928.0	94.5	4766		0.257	1.240	0.000	0.000
Tango	3 W	5395.9	73.5	4936		0.323	1.559	0.000	0.000
Tango	Total	39857.7	199.6	18931		0.130	0.627	1.434	0.900
Echo	1 N	89.3	9.4	267	2.7	2.088	10.083	0.268	0.113
Echo	1 C	89.3	9.4	244	9.3	2.088	10.083	0.922	0.356
Echo	1 S	89.3	9.4	250		2.088	10.083	0.000	0.000
Echo	2 N	916.1	30.3	980		0.724	3.494	0.000	0.000
Echo	2 C	985.6	31.4	894		0.700	3.380	0.000	0.000
Echo	2 S	985.6	31.4	916		0.700	3.380	0.000	0.000
Echo	3 N	192.3	13.9	445		1.472	7.110	0.000	0.000
Echo	3 C	192.3	13.9	406		1.472	7.110	0.000	0.000
Echo	3 S	175.0	13.2	416		1.537	7.423	0.000	0.000
Echo	4 N	268.9	16.4	446		1.264	6.104	0.000	0.000
Echo	4 S	636.2	25.2	1110		0.854	4.125	0.000	0.000
Echo	5 SP1	101.8	10.1	80		1.967	9.499	0.000	0.000
Echo	5 SP2	142.0	11.9	113		1.690	8.162	0.000	0.000
Echo	Total	6088.5	78.0	6375		0.306	1.475	0.318	0.469

Table 11. Antimony *MASC* values for Tango and Echo Ranges.

Range	Sampling Grid ID	Length Parallel to GW Flow Squared (m^2)	Length Parallel to GW Flow (m)	Area of sampling grid (m^2)	Measured Concentration (mg/kg)	*MASC* (mg/kg)	*MASC* (depth corrected) (mg/kg)	Meas/*MASC*	Area-weighted measured concentration (mg/kg)
Tango	1 E	2544.6	50.4	1180		166	200	0.000	0.000
Tango	1 C-N	635.4	25.2	575	1.7	312	377	0.005	0.052
Tango	1 C-S	574.0	24.0	650	1.9	327	394	0.005	0.065
Tango	1 W	2232.0	47.2	1328	0.83	176	212	0.004	0.058
Tango	2 E	248.3	15.8	305		478	578	0.000	0.000
Tango	2 C	248.3	15.8	306		478	578	0.000	0.000
Tango	2 W	248.5	15.8	306		478	577	0.000	0.000
Tango	3 E	12174.4	110.3	4578		81	98	0.000	0.000
Tango	3 C	8928.0	94.5	4766		94	113	0.000	0.000
Tango	3 W	5395.9	73.5	4936		118	142	0.000	0.000
Tango	Total	39857.7	199.6	18931		47	57	0.003	0.175
Echo	1 N	89.3	9.4	267		762	921	0.000	0.000
Echo	1 C	89.3	9.4	244		762	921	0.000	0.000
Echo	1 S	89.3	9.4	250		762	921	0.000	0.000
Echo	2 N	916.1	30.3	980		264	319	0.000	0.000
Echo	2 C	985.6	31.4	894		255	308	0.000	0.000
Echo	2 S	985.6	31.4	916		255	308	0.000	0.000
Echo	3 N	192.3	13.9	445		538	649	0.000	0.000
Echo	3 C	192.3	13.9	406		538	649	0.000	0.000
Echo	3 S	175.0	13.2	416		561	678	0.000	0.000
Echo	4 N	268.9	16.4	446	1.5	461	557	0.003	0.105
Echo	4 S	636.2	25.2	1110	3.8	312	376	0.010	0.662
Echo	5 SP1	101.8	10.1	80	0.86	718	867	0.001	0.011
Echo	5 SP2	142.0	11.9	113	0.75	617	745	0.001	0.013
Echo	Total	6088.5	78.0	6375		111	135	0.006	0.791

Table 12. 2-4-DNT *MASC* values for Tango and Echo Ranges.

Range	Sampling Grid ID	Length Parallel to GW Flow Squared (m^2)	Length Parallel to GW Flow (m)	Area of sampling grid (m^2)	Measured Concentration (mg/kg)	*MASC* (mg/kg)	*MASC* (depth corrected) (mg/kg)	Meas/*MASC*	Area-weighted measured concentration (mg/kg)
Tango	1 E	2544.6	50.4	1180		9.84	11.88		
Tango	1 C-N	635.4	25.2	575		18.51	22.35		
Tango	1 C-S	574.0	24.0	650		19.39	23.41		
Tango	1 W	2232.0	47.2	1328		10.45	12.62		
Tango	2 E	248.3	15.8	305		28.40	34.29		
Tango	2 C	248.3	15.8	306		28.40	34.29		
Tango	2 W	248.5	15.8	306		28.39	34.27		
Tango	3 E	12174.4	110.3	4578		4.83	5.83		
Tango	3 C	8928.0	94.5	4766		5.56	6.71		
Tango	3 W	5395.9	73.5	4936		6.99	8.44		
Tango	Total	39857.7	199.6	18931		2.81	3.40		
Echo	1 N	89.3	9.4	267		45.24	54.62		
Echo	1 C	89.3	9.4	244		45.24	54.62		
Echo	1 S	89.3	9.4	250		45.24	54.62		
Echo	2 N	916.1	30.3	980		15.67	18.92		
Echo	2 C	985.6	31.4	894		15.16	18.30		
Echo	2 S	985.6	31.4	916		15.16	18.30		
Echo	3 N	192.3	13.9	445		31.90	38.51		
Echo	3 C	192.3	13.9	406		31.90	38.51		
Echo	3 S	175.0	13.2	416		33.30	40.21		
Echo	4 N	268.9	16.4	446		27.39	33.06		
Echo	4 S	636.2	25.2	1110		18.50	22.34		
Echo	5 SP1	101.8	10.1	80		42.62	51.46		
Echo	5 SP2	142.0	11.9	113		36.62	44.22		
Echo	Total	6088.5	78.0	6375		6.62	7.99		

3.5 Uncertainty in Results

The fate and transport assessment models used to derive *MACS* are approximations and simplifications of very complex systems. Therefore, the results from these models are subject to a considerable amount of uncertainty. In this context, there are two types of uncertainty to consider.

- Errors in the model formulation in that the model is a simplification of complex systems that are incompletely understood and inadequately characterized
- Errors in the model input parameters.

The first item cannot be addressed without comparing model predictions with field measurements. Unfortunately, this is difficult, if not impossible to do because model predictions go out tens of hundreds of years and measurements in the future cannot obviously be obtained. The second item can be addressed through parametric uncertainty analysis. Parametric uncertainty analysis is not a statement about the accuracy of the model. Rather, is provides some insight into the precision of a model given the fact that inputs to the model are not well known or are uncertain.

To address the parametric uncertainty of the MASCs, a Monte Carlo simulation was performed using the built-in Monte Carlo routine in GWSCREEN. The output from the Monte Carlo simulation was a

distribution groundwater concentration for a 1 mg source. Using this information, a *distribution* of *MASC* values were calculated. The distribution of *MASC* values (instead of a single deterministic value) can then be incorporated into a decision-making process regarding cleanup, monitoring, or no action.

The Monte Carlo simulation was run for lead and nitroglycerin and the results are illustrated in Figures 11 and 12. Table A-1 in Appendix A lists the input distributions. The graphs may be interpreted as follows:

The **green** shaded area represents MACS values on the lower end of the cumulative frequency distribution (≤ 5%). These values may be considered a cutoff value for no action. That is, if the soil concentration for a source of length *L* falls within the greed shaded area or less, then the no further action may be required

The **blue** shaded area represents MACS values in the lower-middle portion of the cumulative frequency distribution (5%> and < 50%) and may be considered the range of values where monitoring may be suggested depending on the circumstances.

The **yellow** shaded area represents MACS values in the upper middle portion of the cumulative frequency distribution (50%> and < 95%) and may be considered the range of values where monitoring may be required depending on the circumstances.

The **red** shaded area represents MACS values on the upper end of the cumulative frequency distribution (≥95%) and would indicate soil concentrations where cleanup or remediation would be required.

It should also be noted that in all cases, the Kd value was the most sensitive parameter accounting for over 90% of the variability in the model output. The other important parameters were the infiltration rate (3.3% of the variability), dispersivity in the unsaturated zone (1.37%), pore velocity in the aquifer (2.98%), and vertical dispersivity (1.4%).

W may apply this methodology to nitroglycerin at the Tango 1 C-N sampling region. The length of the region parallel to groundwater flow was 78.6 ft (see Table 10) which when converted to meters and squared is 635 m^2. Looking up the *MACS* value in Figure 12 for a length squared value of 635 m^2 gives the following approximate values for a 0.3048 m thick source

	0.3048 m thick source	0.076 m source
No Action:	< 1.8 mg/kg	<6.9 mg/kg
Monitoring	>1.8 mg/kg and <22 mg/kg	>6.9 mg/kg and <88 mg/kg
Clean-Up	>22 mg/kg	>88 mg/kg

The values on the right have been corrected to a 0.076 m source. The measured concentration of 26 mg/kg falls within the recommended monitoring range for the 0.076 m thick source. Therefore, one possible solution to exceeding the nitroglycerin MASC value is to require nitroglycerin monitoring instead of demanding remediation.

The example application is not intended to be definitive and changes in the parameter distributions will change the output distribution. Nevertheless, this example demonstrates how parametric uncertainty analysis may be used to define soil concentration levels that trigger given responses. These trigger levels incorporate the uncertainty in the model and provide flexibility in terms of implementing best management practices.

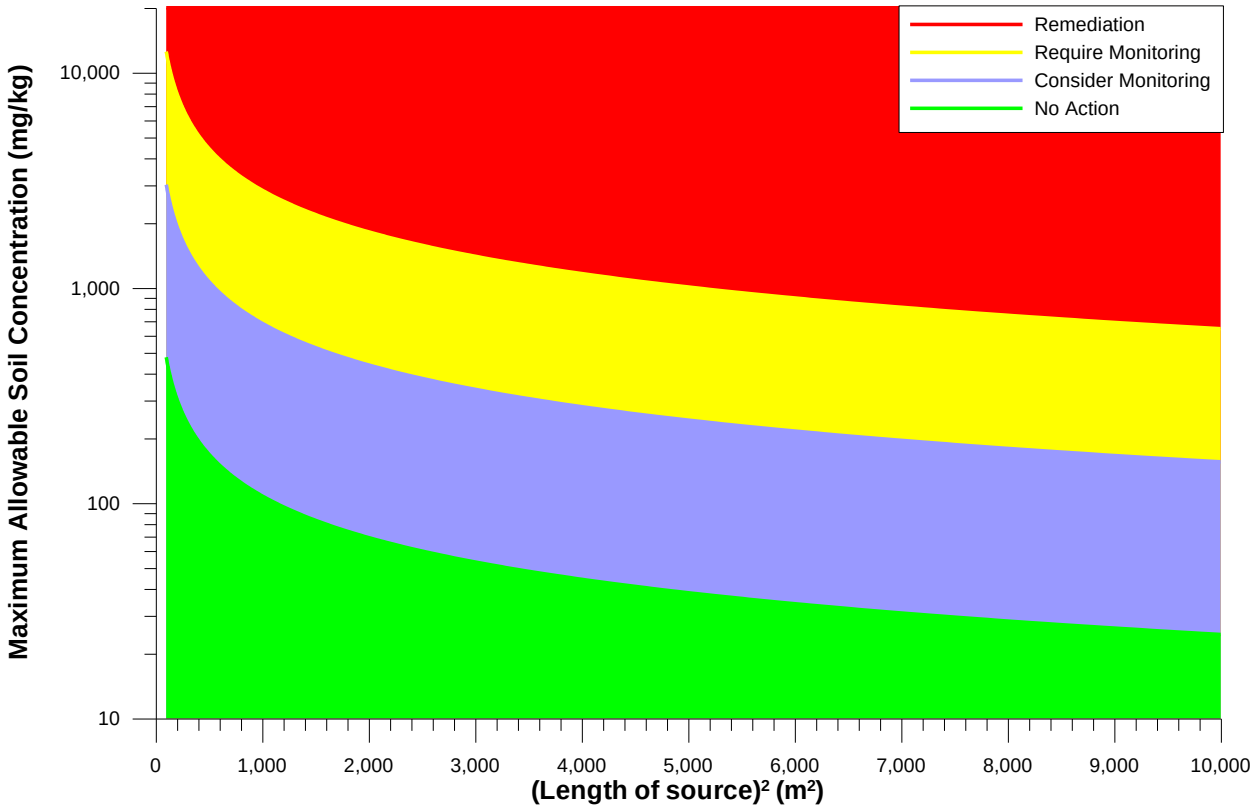

Figure 11. Distribution of lead MASC values as a function of the square length of the source parallel to groundwater flow.

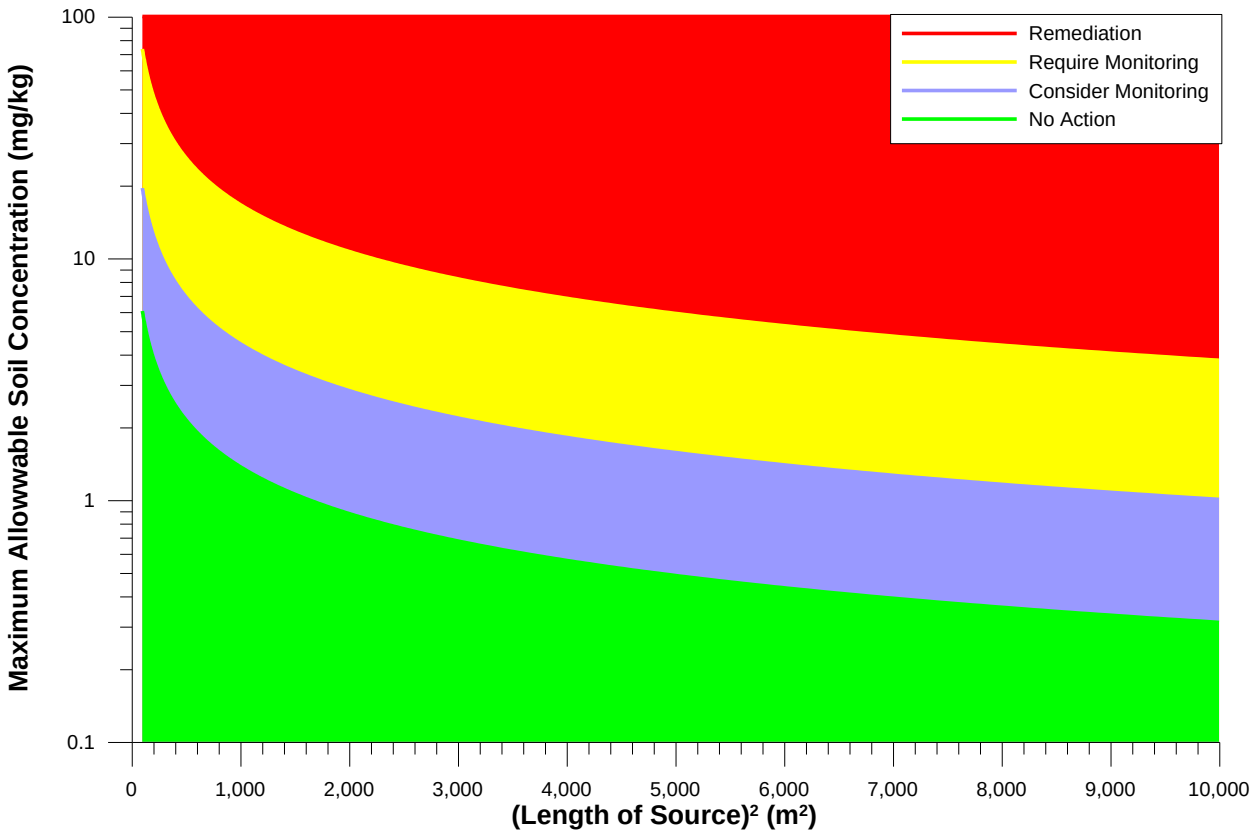

Figure 12. Distribution of nitroglycerin MASC values as a function of the square length of the source parallel to groundwater flow.

3.6 Recent Developments on the Fate of Nitroglycerin

Explosives compounds are released to the environment at military test ranges, mainly near the line of fire, but also in the impact area, if combustion is not complete. The environmental fate of the organic explosive residues varies widely (Brannon et al.2004). Microbial degradation of the organic explosive residue plays an important role in the environmental fate. Nitroglycerin metabolism follows a series of denitration steps, and is eventually mineralized to carbon dioxide (Figure 13). The degradation intermediates (glycerols), may have different fate in the environment than nitroglycerin. A study conducted by Yost (2004) provides data from which the fate of nitroglycerin in soils can be deduced.

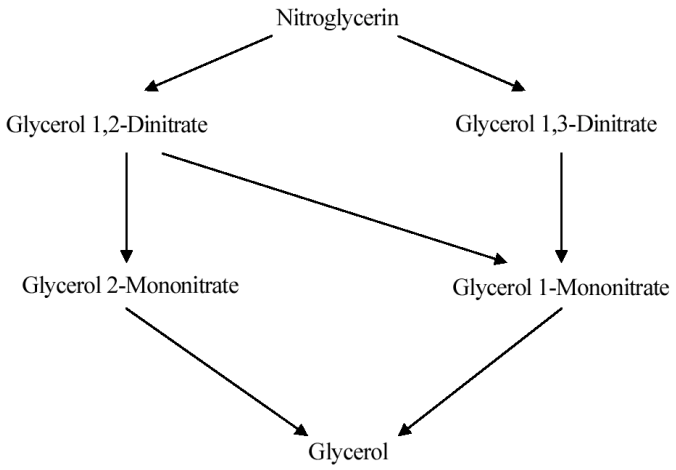

Figure 13. Biodegradation pathway for nitroglycerin. Glycerol is subsequently mineralized to CO_2 (Yost 2004).

Yost investigated the biodegradation of nitroglycerin in soil suspensions as a function of pH and redox potential using batch experiments. Reaction vessels were filled with water, soil, and nutrients, and allowed to incubate for 14 days at set pH and redox conditions. The microbial communities in the system were therefore, given time to stabilize. The reaction vessels were then spiked with nitroglycerin. Over the next 7 days, samples of the solution were extracted, and analyzed for dissolved nitroglycerin.

The microbial communities were not characterized, and so differences in quantities and types of bacteria between the two soils are not known. Also, no abiotic or sterile controls were run, so the possibility of abiotic transformation of nitroglycerin cannot be evaluated. Also, sorption cannot be differentiated from degradation in the batch experiments because degradation products were not quantified.

The three variables examined in this study were soil type, pH, and redox potential. The pH was buffered at one of three values, 6, 7, or 8. Two soils were used, a near surface soil that contained about 2.4% organic carbon, and an aquifer soil that contained 0.2% organic carbon. The surface soil also had somewhat higher cation exchange capacity, but this should have little effect on nonpolar organic compounds. The redox potential in the oxidized experiment was 500 mV, which is in the stability field of NO_3^- (Figure 14). The reduced experiment was conducted at -150 mV, which is in the stability field of NH_4^+. This difference in redox potentials covers a potentially significant range of redox conditions relevant for nitrogen species in water.

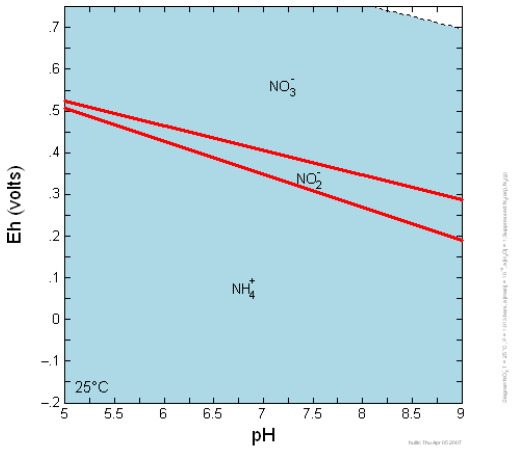

Figure 14. Speciation of nitrogen in water as a function of pH and Eh.

Based on figures presented in Yost (2004), neither soil type nor pH have little effect on the removal of nitroglycerin. Note that all that was measured in these experiments was the aqueous concentration of nitroglycerin. It is not known if nitroglycerin is degraded or simply adsorbed to the soil organic matter. Redox potential, did have a significant effect on nitroglycerin removal from solution. In the reduced environment, nitroglycerin was completely removed from solution within 24 hours. In the oxidized experiments, nitroglycerin removal was still complete, but required 3 to 5 days. Therefore, some combination of biodegradation and adsorption quantitatively remove nitroglycerin within a few days.

To further define the fate of the nitroglycerin, a series of mass balance experiments was conducted using nitroglycerin labeled with ^{14}C. By measuring the distribution of ^{14}C in the system, the fate of nitroglycerin might be better defined. In these experiments, the discharge line from the reaction vessel was passed through a high pH solution of potassium hydroxide. Any carbon dioxide released from mineralization of the nitroglycerin would be trapped in the potassium nitrate solution. At the end of the experiments, ^{14}C distribution was measured for the CO_2 generated, the aqueous phase in the reaction vessel, and the solid phase in the reaction vessel. The mass balance experiments were run for 14 days. Therefore, all of the nitroglycerin had time to be removed from solution, based on the results from the batch experiments.

There are three potential reservoirs in the mass balance experiments: the aqueous phase in the reaction vessel, attached to soil in the reaction vessel, and mineralized to CO_2. Nitroglycerin was completely removed from the aqueous phase in the batch experiments within 5 days. Any ^{14}C in carbon dioxide will be swept out of the reaction vessel and trapped in the potassium hydroxide solution. Therefore, we can conclude that any ^{14}C remaining in the aqueous phase is present in the form of nitroglycerin degradation intermediates. The ^{14}C in the CO_2 represents complete mineralization of the nitroglycerin. What is not clear is what compound contains the ^{14}C associated with the solid soil material in the experiments. This can either be nitroglycerin, or nitroglycerin degradation products.

The mass balance experiments show that soil type is the most important factor in controlling the distribution of the ^{14}C at the end of the experiment (Figure 15). The key difference between the two soils may be the amount of organic carbon. If organic carbon in the soil serves as a sorption media for either the nitroglycerin, or the nitroglycerin degradation intermediates, then a difference in the distribution of ^{14}C between the two soils based on organic carbon content could be explained. If nitroglycerin were the compound being sorbed, then the batch experiments should have shown some difference between the two soils, but did not. Based on this, it seems that the degradation intermediates are being sorbed to the

organic matter in the soil. This is further substantiated by the high fraction of ^{14}C remaining in aqueous solution in the aquifer soil mass balance experiment (low organic carbon content) presumably associated with no aqueous phase nitroglycerin.

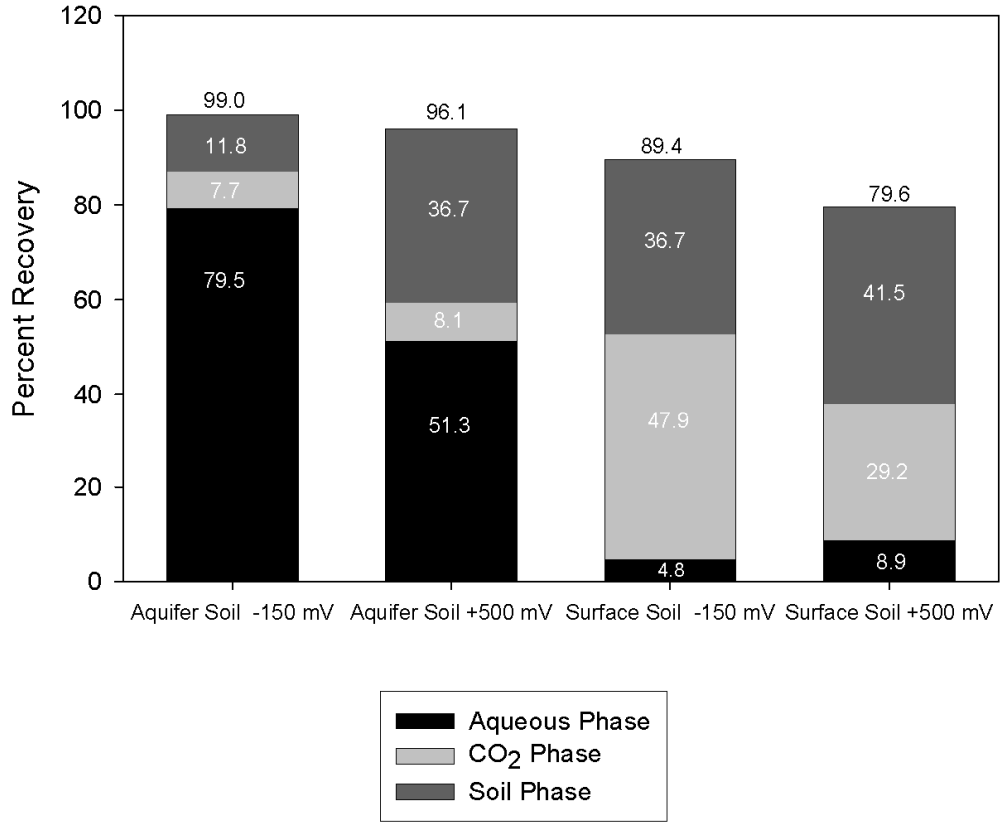

Figure 15. Results of mass balance experiment showing the distribution of ^{14}C among three reservoirs: aqueous phase, sorbed phase, and mineralized CO_2.

Based on these experiments, the following conceptual model for the degradation of nitroglycerin in soil - water systems is proposed (Figure 16). Nitroglycerin is rapidly removed from solution. We identify this step as biodegradation in the conceptual model because a large amount of ^{14}C remains in the aqueous phase in the mass balance experiments for the low-organic-matter soil. When there is little organic matter in the soil, the degradation residuals remain in solution, and would potentially be mobile in the environment. When the soil has sufficient organic matter, the degradation intermediates are sorbed to the soil organic matter. We identify addition biodegradation of the degradation intermediates associated with the sorbed organic matter because there is very little generation of CO_2 gas for the low organic matter soil and quite a bit of CO_2 generation for the high-organic-matter soil. If the soil has several percent total organic carbon, then the degradation intermediates seem to be sorbed. A significant fraction of this sorbed material is further degraded to CO_2.

From these experiments, the rate of nitroglycerin biodegradation is very rapid. Even in oxidized soils, nitroglycerin should be degraded within a few days. The degradation intermediates, however, are stable in aqueous solution for a much longer period (up to a week in this experiment). The intermediates do not seem to be subject to biodegradation in the aqueous phase. Therefore, the degradation intermediates are

much more likely to be mobile and to migrate downwards to groundwater. If the soil has sufficient organic matter, the degradation intermediates will be sorbed to the soil organic matter. In this case, the intermediates will be much less mobile. Biodegradation of the intermediates sorbed to soil organic matter is a much slower process than nitroglycerin degradation in solution. While nitroglycerin was biodegraded within a few days, only about half of the sorbed degradation intermediates were mineralized to CO_2 within a week.

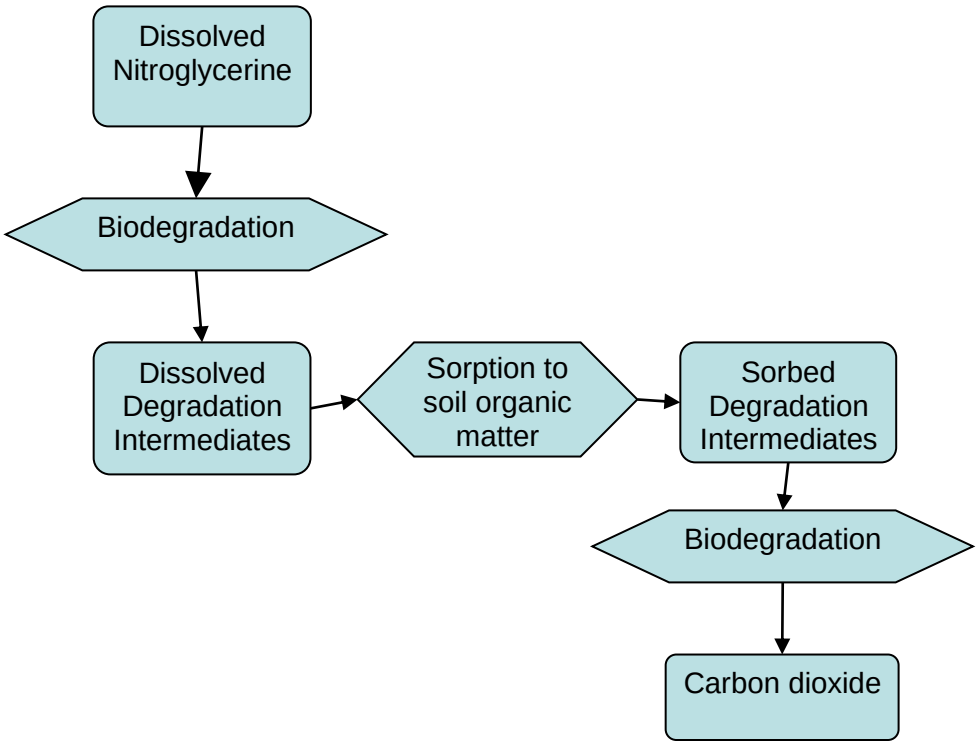

Figure 16. Conceptual model of nitroglycerin degradation in laboratory batch biodegradation experiments.

Generally, these experiments support the conclusion that nitroglycerin will not persist in the soil environment for more than a few days. The fate of the degradation intermediates is more variable, however, and depends on the organic carbon content of the soil. In soils with high organic carbon content, the degradation intermediates will be sorbed and eventually mineralized. However, in soils low in dissolved organic carbon, the degradation intermediates seem to be stable, and available for downward migration to groundwater.

To test this conceptual model by field sampling, soil samples should be collected at multiple depths in the soil column. The soil should be extracted to assure that any analyte sorbed to soil organic carbon is extracted and included in the analysis. Both nitroglycerin and the degradation intermediates should be measured. The soil organic carbon content should also be determined. Sampling at multiple depths and for both nitroglycerin and the degradation intermediates will determine if the intermediates are mobile and could migrate to groundwater.

3.6.1 Incorporating Dissolution and Biodegradation

Figure 17 is an idealized conceptual model for soil partitioning and dissolution processes for a generic contaminant in soil. A contaminant (such as lead or nitroglycerin) is deposited on the soil surface from the weapons training. Some of this contaminant readily dissolves in water and the remainder stays in an un-dissolved form. The fraction that dissolves then goes through equilibrium sorption reactions. A fraction of it goes to pore water and a fraction of it sorbs to soil particles. (The ratio of the concentration in pore water and the concentration sorbed to soil particles is the Kd value.) The fraction in pore water can then be transported to groundwater.

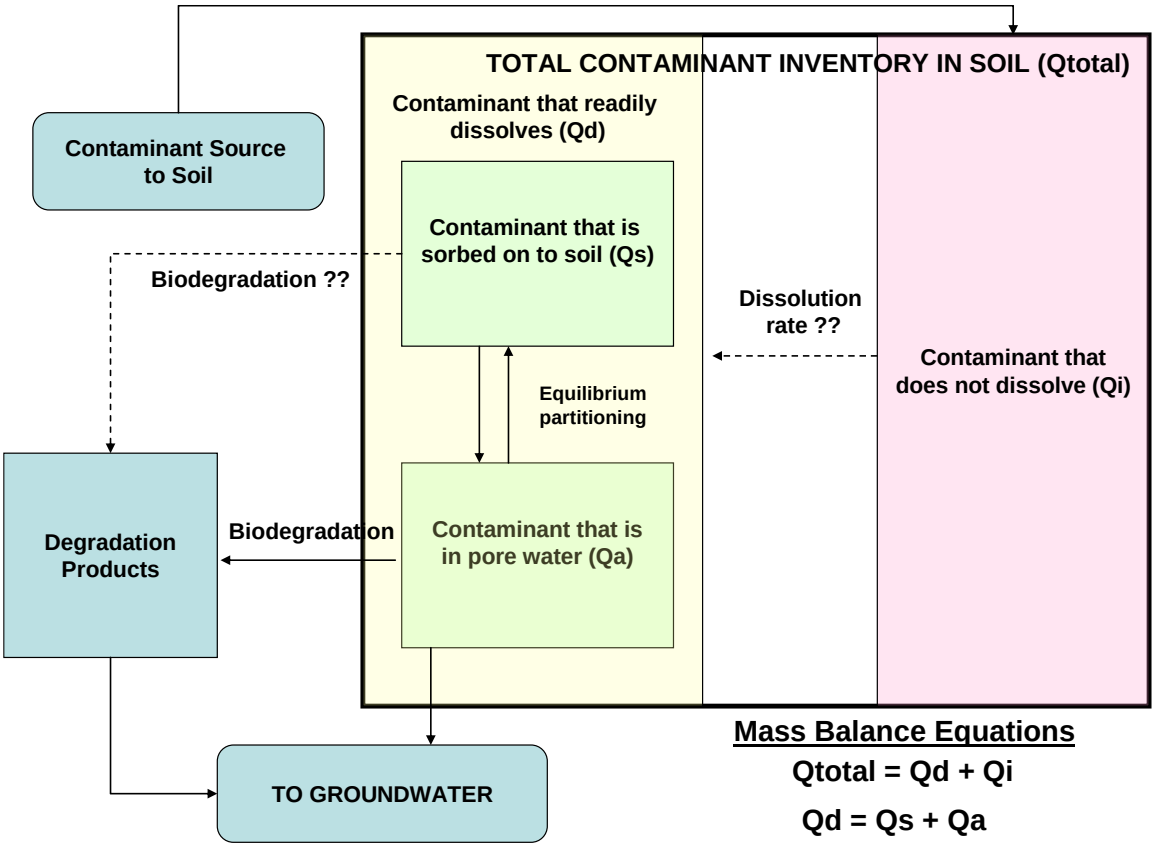

Figure 17. Conceptual model for contaminant dissolution, aqueous partitioning, and biodegradation in soil.

Biodegradation may reduce the contaminant mass in either the sorbed or aqueous phases. This process is not relevant for a metal such as lead, but was shown to be important for nitroglycerin, and could be for other organic compounds. Note the mass balance equations in the lower left corner of the figure. The total contaminant inventory in soil is made up of the inventory of contaminant that will readily dissolve and the inventory that is insoluble. Of the inventory that readily dissolves, there is a fraction that sorbs to soil and a fraction that remains in pore water. Of the inventory in the insoluble form, there is a rate at which it transforms from an insoluble to soluble form and shown in Figure 17 as the dissolution rate.

Both SESOIL and MCM models assume all the contaminant present in the soil will readily dissolve in pore water until the solubility limit of the contaminant is reached. Therefore, the box that is labeled "Contaminant that does not dissolved" is not considered, and all the contaminant that is in the soil is

assumed to readily dissolve. Therefore, the MASC values calculated from SESOIL and MCM really only apply to contaminants that are in a readily dissolvable phase.

Both models also assume equilibrium partitioning using the Kd value. This is a simplistic representation of reality because geochemical conditions that can vary both spatially and temporally determine the partitioning between aqueous and sorbed phases of the contaminant. Additional modeling work can be done using geochemical models. This work should be used to try to understand the overall impact of geochemical conditions on the sorption process. However, it is not practical to establish MASC values using a geochemical model because geochemical conditions vary too much and cannot be quantified temporally and spatially with any certainty. Rather, the results of a geochemical model can be used to modify the Kd value used, and compute MASC values using either SESOIL or MCM.

Another option is to compute fluxes to the vadose zone from the surface soil using an external model derived from the conceptual model illustrated in Figure 17. The mathematical model assumes all processes can be approximated by first order reactions and equilibrium reversible sorption. The following differential equations may be written that describe the mass balance of contaminant in the surface soil.

$$\frac{dQI}{dt} = R - \lambda_d QI$$

$$\frac{dQD}{dt} = \lambda_d QI - \lambda_{BA}\frac{QD}{Rd} - kQD - \lambda_{BS}QD(1 - 1/Rd) \quad (8)$$

Where

QI = contaminant inventory in the insoluble phase (g)

R = the rate of deposition of the contaminant in the insoluble phase (g yr^{-1})

λ_d = dissolution rate constant (yr^{-1})

QD = contaminant inventory in the dissolved phase (g)

λ_{BA} = biodegradation rate constant for dissolved phase contaminant (yr^{-1})

λ_{BS} = biodegradation rate constant for sorbed-phase contaminant (yr^{-1})

k = leach rate constant ($I/(\theta\, Rd\, T)$, yr^{-1})

Rd = retardation factor ($1 + Kd\, \rho/\theta$)

I = infiltration rate (m yr^{-1})

θ = moisture content

Kd = linear sorption coefficient ($m^3\ g^{-1}$)

ρ = bulk density (g m^{-3})

T = soil layer thickness (m)

The solution to Equation 8 for the boundary conditions $R = 0$ for all t, and initial conditions $QI=QI_0$ at $t = 0$ is

$$QI(t) = QI_o e^{-\lambda_d t}$$
$$QD(t) = \frac{\lambda_d QI_o}{\lambda_d - (k + k_e)}\left[e^{-(k+ke)t} - e^{-\lambda_d t}\right] \quad (9)$$
$$k_e = \frac{\lambda_{BA}}{Rd} + \lambda_{BS}\left(1 - 1/Rd\right)$$

The contaminant flux to the vadose zone from the surface soil is estimated by $kQD(t)$. Equation 9 can be implemented in a spreadsheet, output to an ASCII file, and be read into MCM or SESOIL as an external source.

4. REFERENCES

AMEC, 2001. DRAFT Contaminant of Concern Identification Demolotion Area 1-Soil Operable Unit. MMR-3254, AMEC Earth and Environment Inc., 239 Litteton Road, Siute 1B. Westford, Massachusetts.

AMEC Earth and Environment , 2004. *Draft Human and Ecological Work Plan.* Camp Edwards, Massachusetts Military Reservation.

Brannon, J. M., J. C. Pennington, S. Yost, and C. Hayes, 2004, "Fate and transport of explosives", *Proceedings of the First Conference on Sustainable Range Management*, New Orleans, LA, Jan 5-8 2004, 1124-1145.

Carsel, R. F. and R. S. Parrish, 1988, Developing joint probability distributions of soil water retention characteristics *Water Resources Research*, 25(5), 755–769.

EPA 2004. *ProUCL Version 3.0 User Guide*. EPA/600/RO4/079. U.S. Environmental Protection Agency, Washington DC.

Jacques, D. and Simunek, J. (2005). *User manual of the multicomponent variably-saturated flow and transport model HP1*. SCK-CEN-BLG-998. Belgian Nuclear Research Centre. Mol, Belgium.

Larson et al. 2007. (In Progress). *Geographical Comparison of Partition Coefficients for Metals Associated with Military Munitions*.

Parkhurst, D.L. and Appelo, C.A.J. (1999). *User's guide to PHREEQC (version 2) - a computer program for speciation, batch-reaction, one-dimensional transport, and inverse geochemical calculations*. U. S. Geological Survey. Denver, Colorado.

Rood, A. S., 1999, *GWSCREEN: A Semi-Analytical Model for Assessment of the Groundwater Pathway from Surface or Buried Contamination, Theory and User's Manual*, Version 2.5. INEEL/EXT-98-00750, Idaho National Engineering and Environmental Laboratory, 1999.

Rood, A.S., 2004. "A Mixing-Cell Model for Assessment of Contaminant Transport in the Unsaturated Zone Under Steady-State and Transient Flow Conditions." *Environmental Engineering Science*, 21(6).

Rood, A.S., 2005. *Mixing Cell Model: A One-Dimensional Numerical Model for Assessment of Water Flow and Contaminant Transport in the Unsaturated Zone*. ICP/EXT-05-00748 Rev 0, Idaho National Laboratory, Idaho Falls ID January.

Rood, A.S., and L.C. Hull 2007. *Review of Environmental Assessment of Lead at Camp Edwards Massachusetts Small Arms Ranges and Calculation of Maximum Lead Concentrations in Soil for Protection of Groundwater*. Informal Technical Memo to EPA Region 1 from Idaho National Laboratory, February 5, 2007.

Rood, A.S., 2007. *Some Comments Pertaining to Modeling Issues Discussed at the February 15th, 2007 Meeting on Modeling for Small Arms Ranges Tango and Echo*. Informal Memo to EPA Region 1 from Idaho National Laboratory, February 20, 2007.

Simunek, J., Sejna, M. and van Genuchten, T. (1998). *The HYDRUS-1D software package for simulating the one-dimensional movement of water, heat, and multiple solutes in variably-saturated media*. IGWMC-TPS 70. U. S. Salinity Laboratory, U. S. Department of Agriculture. Riverside, CA.

Toride, N., Leij, F.J. and van Genuchten, M.T. (1995). *The CXTFIT code for estimating transport parameters from laboratory or field tracer experiments, version 2.0*. Research Report No. 137. U. S. Salinity Laboratory, Agricultural Research Service. Riverside, CA.

USACE (U.S. Army Corps of Engineers) 2006a. *T Range Soil and Groundwater Investigation Report*. U.S. Army Corps of Engineers, New England District, Concord Massachusetts.

USACE 2006b. *E Range Soil and Groundwater Investigation Report*. U.S. Army Corps of Engineers, New England District, Concord Massachusetts.

van Genuchten, M. Th., 1980, "A Closed-form Equation for Predicting the Hydraulic Conductivity of Unsaturated Soils," *Soil Sci. Soc. Am J*., 44, 892–898.

Whelen, G., J.P. McDonald, C. Sato., 1996. *Multimedia Environmental Assessment System (MEPAS): Groundwater Pathway Formulations.* Pacific Northwest National Laboratory, Richland Laboratory, Richland Washington.

Yost, S., 2004, *Effects of Redox Potential and pH on the Fate of Nitroglycerin in a Surface and Aquifer Soil*, M. S. Thesis, Louisiana State University, Baton Rouge, LA.

Table A-1 Parameter distributions used in Monte Carlo Simulation.

Table A-1. Parameter Distributions used in Monte Carlo simulation for lead and nitroglycerin

Distribution	Parm1	Parm2	Parm3	Parm4
Triangular	min	mode	max	
Lognormal	GM	GSD	min	max
Uniform	min	max		

Parameter	GWSCREEN Variable	Distribution Type	Determininistic Value	Parm1	Parm2	Parm3	Parm4	notes
Infiltration (m/yr)	PERC	triangular	0.7366	0.492049	0.7366	0.981151	n/a	mode value used by the Army, min and max based on 2X the CV determined using std of the annual ppt from the 1970-2005 Blue Hill data
bulk density, source (m/yr)	RHOS	none	1.4					based in Speital and Yamamoto 2002
bulk density, vadose zone (m/yr)	RHOU	none	1.6					based in Speital and Yamamoto 2002
bulk density aquifer (m/yr)	RHOA	none	1.7					based in Speital and Yamamoto 2002
dispersivity in vadose zone (m)	AXU	triangular	1.8	0.9	1.8	3.6	n/a	mode based on Z/40, min Z/20, Max Z/10, Z=36 m
unsaturated thickness (m)	DEPTH	none	37					
darcy velocity in aquifer (m/yr)	U	triangular	37	24	37	50	n/a	Based on Amry model and AMEC 2001
porosity of aquifer	PHI	uniform		0.3	0.4	n/a	n/a	Range of values used by Army and EPA
longitudinal dispersivity (m)	AX	triangular	3	1.5	3	6		Determinsistic value based on data provided by Dave McTigue; distribution assumed +/- a factor of 2
transverse dispersivity (m)	AY	triangular	0.09	0.045	0.09	0.18		Determinsistic value based on data provided by Dave McTigue; distribution assumed +/- a factor of 2
vertical dispersivity (m)	AZ	triangular	9.14E-03	0.00457	9.14E-03	0.01828		Determinsistic value based on data provided by Dave McTigue; distribution assumed +/- a factor of 2
Kd in source (mL/g)	KDS							
	lead	lognormal	47	47	2.6	0.01	1.00E+04	GM and GSD from calibration to soil profiles
	antimony	lognormal	45	45	2.5	0.01	1.00E+04	GM based on Shepperd and Thibault, GSD assumed
	nitroG	lognormal	1.9	1.9	2.5	0.001	100	GM based on Speital and Yamamoto 2002, assumed GSD of 2.5
	24DNT	lognormal	3.2	3.2	2.5	0.001	100	GM based on Speital and Yamamoto 2002, assumed GSD of 2.5
Kd in vadose zone (mL/g)	KDU							
	lead	lognormal	47	47	2.6	0.01	1.00E+04	GM and GSD from calibration to soil profiles
	antimony	lognormal	45	45	2.5	0.01	1.00E+04	GM based on Shepperd and Thibault,

Table A-1. Parameter Distributions used in Monte Carlo simulation for lead and nitroglycerin

Distribution	Parm1	Parm2	Parm3	Parm4
Triangular	min	mode	max	
Lognormal	GM	GSD	min	max
Uniform	min	max		

Parameter	GWSCREEN Variable	Distribution Type	Determininistic Value	Parm1	Parm2	Parm3	Parm4	notes
Kd in aquifer (mL/g)	KDA							
	nitroG	lognormal	0.9692	0.9692	2.5	0.0001	1.00E+04	GSD assumed based on 1/2 difference between surface and subsurface Kd values
	24DNT		1.73	1.73	2.5	0.0001	1.00E+04	based on 1/2 difference between surface and subsurface Kd values
	lead	lognormal	47	47	2.6	0.01	1.00E+04	GM and GSD from calibration to soil profiles
	antimony	lognormal	45	45	2.5	0.01	1.00E+04	GM based on Shepperd and Thibault, GSD assumed
	nitroG	lognormal	0.0384	0.0384	2.5	0.00001	1.00E+02	GM based on Speital and Yamamoto 2002, assumed GSD of 2.5
	24DNT	lognormal	0.26	0.26	2.5	0.00001	1.00E+02	GM based on Speital and Yamamoto 2002, assumed GSD of 2.5